Ceramics International 45 (2019) 4700–4706

Contents lists available at ScienceDirect

Ceramics International

journal homepage: www.elsevier.com/locate/ceramint

Molecular dynamics simulation and experimental verification for bonding formation of solid-state TiO_2 nano-particles induced by high velocity collision

Hai-Long Yao[a,b], Guan-Jun Yang[a,*], Chang-Jiu Li[a,*]

[a] State Key Laboratory for Mechanical Behavior of Materials, School of Materials Science and Engineering, Xi'an Jiaotong University, Xi'an 710049, Shanxi, China
[b] Jiangxi Province Engineering Research Center of Materials Surface Enhancing & Remanufacturing, School of Mechanical and Materials Engineering, Jiujiang University, Jiujiang 332005, Jiangxi, China

ARTICLE INFO

Keywords:
Chemical bonding
Atomic displacement
MD simulation
HR-TEM
Nano-ceramic particle

ABSTRACT

Collision processes of solid-state nano-sized ceramic particles were investigated by molecular dynamics (MD) simulation in order to clarify their bonding mechanisms. Effect of particle temperature on particle bonding formation was examined, and collision behavior of nano-sized TiO_2 particle was discussed in terms of particle deformations. Microstructures and bonding qualities of bonded nano-sized TiO_2 particles induced by high velocity collision were examined by high resolution transmission electron microscope (HR-TEM) to verify the MD results. Simulation results demonstrate that the bonding formation of nano-sized TiO_2 particles can be attributed to the atomic displacement and lattice distortion in localized impact region of particle boundaries. TEM microstructure results prove simulation results and indicate effective chemical bonding formations between nano-particles at low temperature by high velocity collision. Quantitative results show that the high temperature is beneficial to the particle bonding formation. The asperity around nano-sized ceramic particles surface contributes to the displacement and lattice distortion in localized impact region under the high impact compressive pressure. The fact demonstrates a new mechanism of nano-scale ceramic particle bonding formation induced by the localized atomic displacement. The study present opens up a promising prospect of fabricating functional equipment with nano-scale ceramic particles with high velocity collision at ambient temperature.

1. Introduction

Inter-particle bonding plays a key role in determining properties of nano-porous materials. Good inter-particle bonding improves their mechanical properties [1–3] and electric properties [1,4,5]. The chemical bonding between nano-particles is mostly created by high-temperature approaches [6–8]. However, most novel functional materials are in metastable structures, which are sensitive to the conventional high-temperature sintering methods [9–11]. Therefore, a high velocity collision process can be used as a complementary approach to bond particles of those metastable materials [1,2]. Metallic particles can be bonded together by the high velocity collision when remaining at the solid phase due to their good plastic deformation abilities. For high velocity collision [2,3,12], adiabatic shears instability occurs to the particle interface, forming chemical bonding interface. However, they are lack in knowledge on the nano-particle bonding between ceramic materials with essential brittle behaviors.

Nano-ceramic materials can also present certain plastic deformation behaviors based on dislocation sliding or twinning. This phenomenon is similar to the plastic deformation of metal. Fine ceramic materials have been shown to exhibit dramatically different deformation behaviors from their bulk counterparts [13–19], although bulk ceramic is brittle and always crushed during high velocity collision [20,21]. It is well known that plastic deformation behaviors for nano-scale ceramic materials are mainly considered to be attributed to the dislocation or twinning mechanism. For example, the plastic deformations of Al_2O_3 particles [22], GaAs nano-rods [17], silica glass nano-fibers [14], calcium aluminum silicate glasses [15], and single-crystal silicon [23] under the conditions of compression, tensile and bending, are attributed to the formation of dislocations. While, the plastic deformations of Al_2O_3 micro-pillars under micro-compression [24], nano-scale body-centered cubic tungsten [25] and nano twinned Ni_3Al [26] are mainly attributed to twinning. Based on the dislocation or twinning mechanism, the formation of a long bonding neck needs the significant

* Corresponding authors.
E-mail addresses: ygj@mail.xjtu.edu.cn (G.-J. Yang), licj@mail.xjtu.edu.cn (C.-J. Li).

https://doi.org/10.1016/j.ceramint.2018.11.162
Received 21 October 2018; Received in revised form 18 November 2018; Accepted 21 November 2018
Available online 22 November 2018

disappearing spherical segment for the two bonded spherical particles around the bonding region. This fact leads to more longitudinal deformation of the particles. However, a “smaller is stronger” trend has been developed for single-crystal materials in micro or nano-scale [27–31]. The sample size is smaller, the stresses required to cause yield and sustain plastic flow is higher. This leads to more difficult for the nucleation and operation of dislocations or twinning. Therefore, if the disappearing spherical segment of the bonded particles is too small to cause the overall deformation of the spherical particles, it is expected that the particle bonding can be formed through some novel mechanism that shows no dependence on dislocation or twinning.

Here the inter-particle bonding formation of nano-sized TiO_2 ceramic particles induced by high velocity collision was investigated. First, molecular dynamics (MD) simulation was carried out to illuminate processes of particle collisions. Microstructures of the bonded TiO_2 ceramic particles were measured using transmission electron microscopy (TEM) and the bonding mechanism of the nano-scale ceramic particles during high velocity collision was discussed.

2. Experimental procedure

2.1. Molecular dynamics simulation for nano-sized TiO_2 particles collision

Molecular dynamics simulation was applied to investigate the particle interface deformation during the collision process of TiO_2 nanoparticles by the Buckingham-type potential [32–34]. Here, charge neutral, two spherical particles with a diameter of 3.8 nm have been cut out from a perfect anatase TiO_2 crystal made of multiples of its unit cells. The applied model consisted of two TiO_2 particles, i.e., a fixed particle and a moving particle (as shown in Fig. 1). Before colliding, these two spherical particles are equilibrated at different temperatures rescaling for 30 ps with a time step of 0.5 fs. Then, quality of equilibration and energy conservation is tested by integration in the microcanonical ensemble (NVE) for additional 10 ps. In order to reproduce the experimental situation, velocity of the gravity center of the fixed particle was adjusted to zero and the moving particle has a negative velocity initially during the MD simulation. The fixed particle is divided into three parts at x-direction: bottom fixed layer of 4 layers, middle constant temperature layer of 11 layers and surface free layer of 6 layers. Collision simulations are carried out for 40 ps in the micro-canonical ensemble (NVE) under the condition of these two particles of an initial temperature of 300 K and the moving particle of an initial velocity of 600 m/s. During collision process, the medium constant temperature layer is maintained at constant temperatures by scaling the velocity of constituting atoms. The temperature of the surface free layer as well as the moving particle is not controlled. This simulation is performed with a minimum separation of 5 nm between the closest boundaries of these separated particles. Collision simulations are

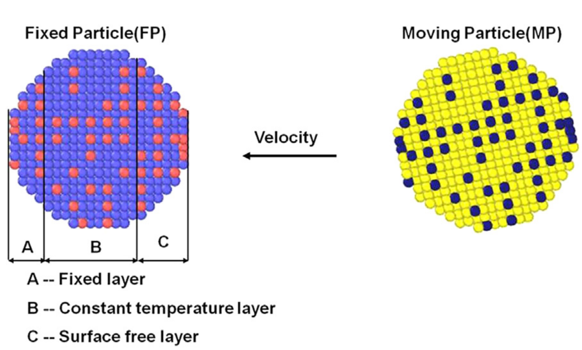

Fig. 1. Collision model for two nano-sized TiO_2 particles.(Blue and yellow atoms refer to O atoms; Red and dark blue atoms refer to Ti atoms). (For interpretation of the references to color in this figure legend, the reader is referred to the web version of this article.)

carried out for 40 ps in the micro-canonical ensemble (NVE) under the condition of these two particles of different temperature and the moving particle initial velocity of 600 m/s. Simulation was implemented by Lammps software on the platform of Intel double cores of linux operation system.

In order to investigate the effect particle temperature on particle bonding formation, the temperature of both the fixed and moving particles were controlled in three terms. One is that both two particles were set 300 K as initial temperature (termed as FP300K-MP300K); another is that the fixed particle was set 300 K as initial temperature, the moving particle was set 773 K as initial temperature (termed as FP300K-MP773K); the least is that both two particles were set 773 K as initial temperature (termed as FP773K-MP773K).

2.2. Microstructure characterization of nano-sized TiO_2 particle bonding

Microstructure of the bonded TiO_2 nanoparticle was investigated to confirm above simulation results. TiO_2 nano-powders (P25, 25 nm, Degussa, Germany) with ambient temperature and 350 °C were deposited to from TiO_2 coating onto an F-doped SnO_2-glass (FTO, TEC-15, LOF) substrate using a lab-developed vacuum cold spray system [35]. For comparison, a screen-printed TiO_2 coating was prepared and sintered at 500 °C for 30 mins, as reported in elsewhere [36]. Microstructures of particle/particle bonding for both the vacuum-cold-sprayed and screen-printed TiO_2 coatings were characterized by transmission electron microscopy (TEM) (JEM-2100F, JEOL, Japan).

3. Results and discussion

3.1. Effect of temperature on particle temperature and particle bonding

Fig. 2 shows effect of temperature on particles temperature during collision. It can be found that the temperature of both particles immediately increased, then decreased to their original temperature. Due to the significant difference in initial temperature between the fixed and moving particles (case B of FP300K-MP773K), the temperature of the moving particle decreased and trend to the original temperature of the fixed particle in case B.

Fig. 3 shows that the neck length of the boned particles was increased by increasing the particle temperature. This result also indicates that the atomic displacements around the compact region were increased with the increase in the particle temperature during collision.

Accordingly, the particle bonding ratio can be measured as $(r/R)^2$, which is equivalent to the contact area ratio. By using the method described above, effect of temperature on the particle bonding ratio can be investigated as shown in Fig. 4. It can be found that the particle bonding ratio of cases of FP300K-MP300K, FP300K-MP773K and FP773K-MP773K was 0.177, 0.194 and 0.233, respectively. The present result was consistent with the result that contact area ratio for the case of in-situ particle heating during cold spraying was higher that of depositing coating at ambient temperature. On the one hand, the MD simulation result confirms that different heating approaches exist in the process of in-situ particle heating during high velocity collision. On the other hand, it clarifies that nano-scale ceramic particles can be bonded together by high velocity collision at ambient temperature.

3.2. Collision behaviors of two impacting TiO_2 particle

Fig. 5 shows a trajectory and snapshots of two impacting TiO_2 particle. The magnitude of the final velocity of the moving particle decreases and becomes around zero, and the distance between the two nanoparticle decreases and tends to be constant, as shown in Fig. 5(a) and (b). Fig. 5(c) shows that two TiO_2 particles were bonded together even though the maximum inverse velocity. By duration of 40 ps, a separation of the two nanoparticles is also never observed over the course of simulation (as shown in Fig. 5(a)). This phenomenon indicates

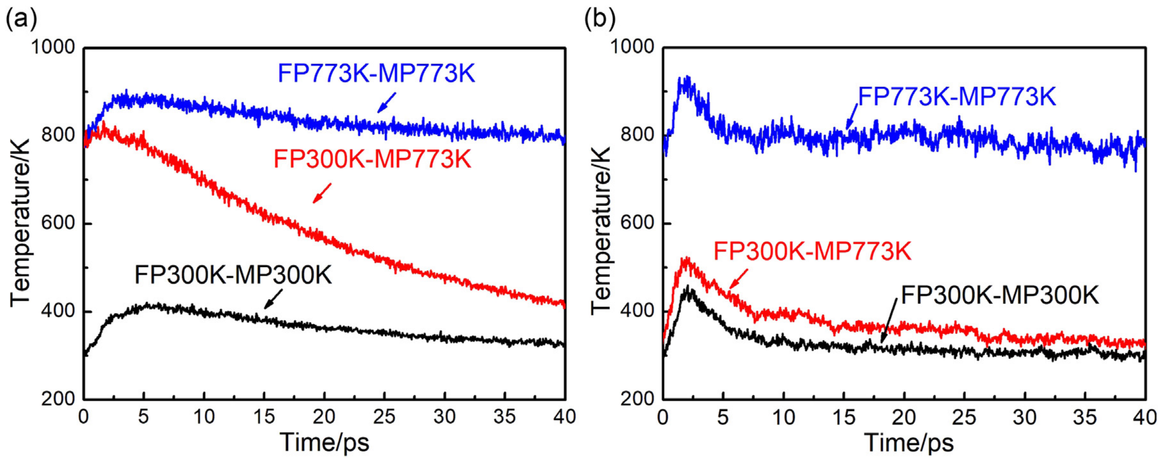

Fig. 2. Effect of heating approach on particle temperature. (a) Temperature of the moving particle; (b) Temperature of the fixed particle. (FP means the fixed particle, and MP means the moving particle.).

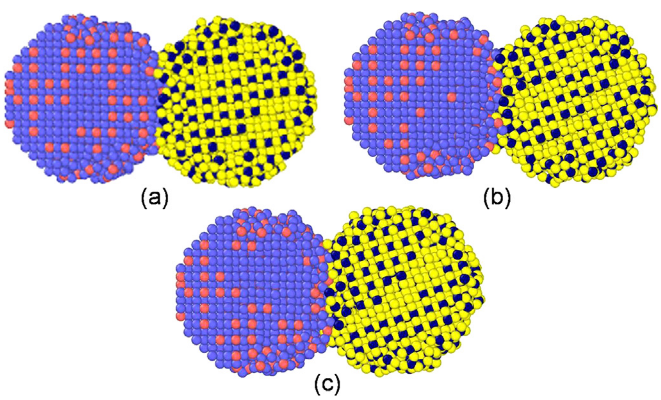

Fig. 3. Configuration of bonded particles with different particle temperature at the impact velocity of 600 m/s.(FP means the fixed particle, and MP means the moving particle). (a) FP300K-MP300K; (b) FP300K-MP773K; (c) FP773K-MP773K. (Blue and yellow atoms refer to O atoms; Red and dark blue atoms refer to Ti atoms). (For interpretation of the references to color in this figure legend, the reader is referred to the web version of this article.)

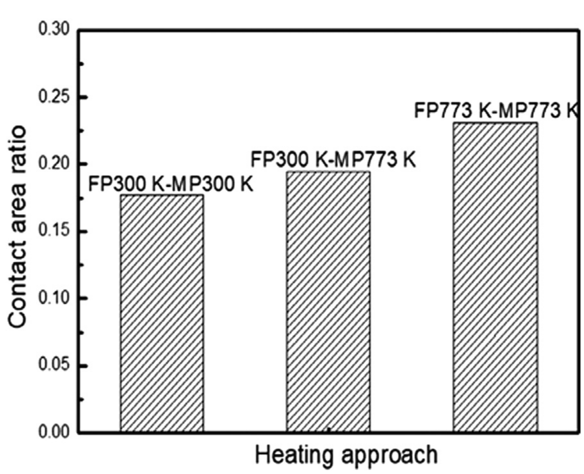

Fig. 4. Effect of heating approaches on particle bonding ratio.

that the two particles are bonded together.

Snapshots in Fig. 5(c) show detailed bonding states. After collision starting, the atoms at the impacting region displace from their original positions, which shows localized atomic displacements. An inter-particle bonding is formed and reaches the maximum when the mass center position reaches the nearest position (1.85 ps in Fig. 5c). Later on, the particles go apart from each other due to rebound accompanied with the mass center velocity being opposite direction. Then two particles reach the farthest position where mass center velocity is zero (3.9 ps in Fig. 5c). We find clearly effective particle bonding is retained, demonstrating that the bonding is not destroyed by rebounding. After that, we further find some oscillations of the particle pair. The particle pair approaches to the equilibrium state owing to the energy dissipation. Finally, particles are accommodated with each other and the bonding neck remains a constant (similar to 40 ps in Fig. 5(c)). By analyzing the atom displacements in the particles around the compact region, only atoms in up to the five layers of the fixed particle and only atoms in up to the three layers of the moving particle exhibit obvious displacements (as shown as 1.85 ps in Fig. 5(c)). Meanwhile, by analyzing the profiles far away from the compact region for the two particles throughout the collision process, atom displacements around the particle profiles are less than a lattice size (as shown in Fig. 5(c)). These characteristics were also observed for the two particles from different directions (as shown in Fig. 5(c)). It is reported that obvious steps can be observed around the materials profiles after dislocation slips [25,37–39]. Those microstructure features in Fig. 5(c) imply that the dislocation slips do not occur throughout the nano-scale TiO_2 particle impact process. It indicates that the bonding formation of TiO_2 nanoparticle is mainly caused by displacing localized atoms in the particles boundaries around the compact regions. The displacement of localized atoms at the particle boundaries appears to be the dominant factor for the TiO_2 bonding formation of these particles scales. This mechanism is completely different from conventional plastic deformation behavior based on dislocation twinning and grain boundary slip [25,37–39]. Compared to the conventional dislocation slip or twinning mechanism, the localized atom displacement mechanism presents a brilliant advantage of no dependence on lattice orientation.

3.3. Microstructures of impacted nano-TiO_2 particles

To further prove this particle bonding mechanism, we examined microstructure of impacted nano-TiO_2 particles with surface modulations of 1–3 nm. For comparison, results of TiO_2 particle pairs sintered at 500 °C were also shown. In TEM images, there have different modes for the interface contact between TiO_2 nanoparticles, including separation, overlapping and effective bonding (as shown in Fig. 6(a)). The overlapped contact mode with Moiré patterns presents a false image of bonding and cannot be applied to judge the property of particle/particle interface contact [40]. Therefore, the reliable characterization of microstructure on the particle/particle interface can be realized by only focusing on the effective bonding mode.

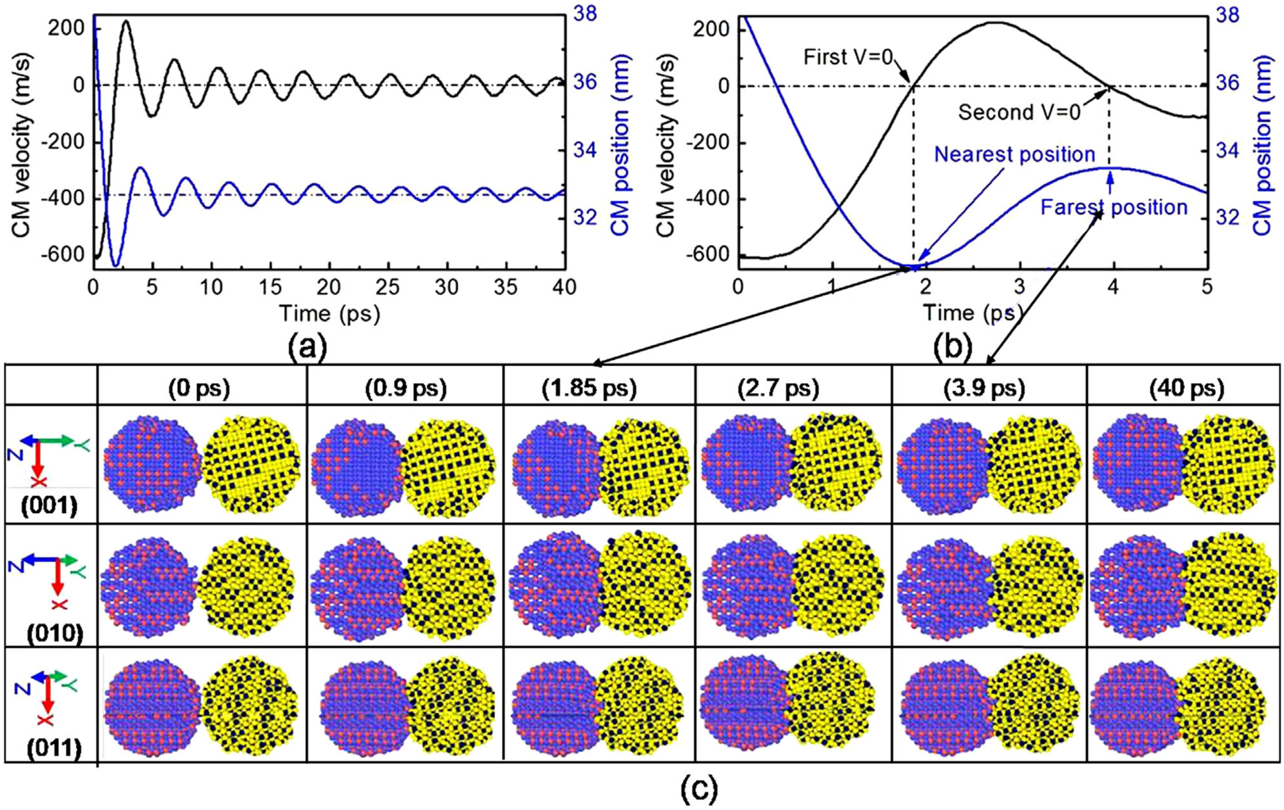

Fig. 5. A trajectory and snapshots of the moving TiO_2 particle colliding with the fixed TiO_2 particle. (a–b) Trajectory of the particles collision; (c) Snapshot of the particles collision for different timesetps. (CM velocity refers to center-of-mass velocity of the moving particle; CM position refers to center-of-mass position of the moving particle. Initial temperature of both moving particle and fixed particle was 300 K and the initial particle velocity was 600 m/s).

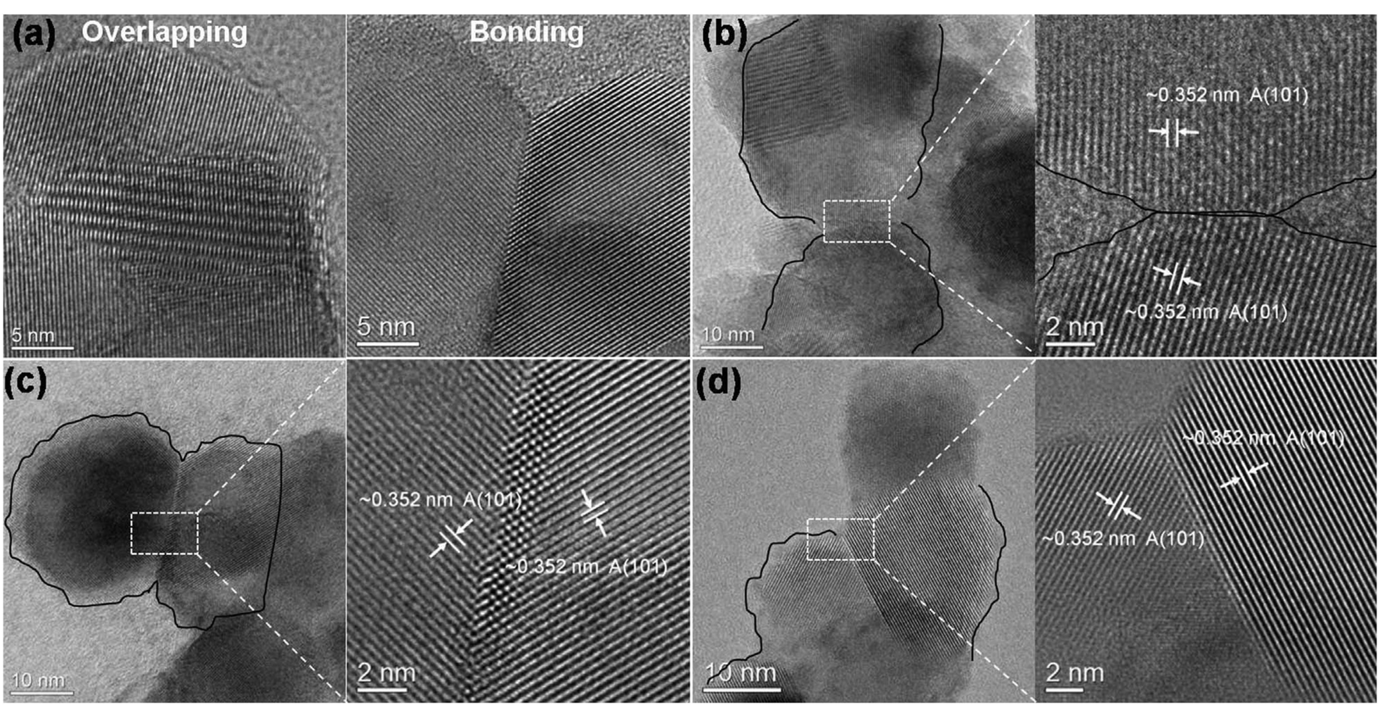

Fig. 6. HR-TEM images of bonded nano-sized TiO_2 particle deposited by different approaches. (a) TiO_2 nanoparticle bonding modes; (b) Vacuum-cold sprayed TiO_2 coating with the particle temperature of RT; (c) Vacuum-cold sprayed TiO_2 coating with the particle temperature of 350 °C; (d) Screen-printed TiO_2 coating with the sintering temperature of 500 °C in 30 min.

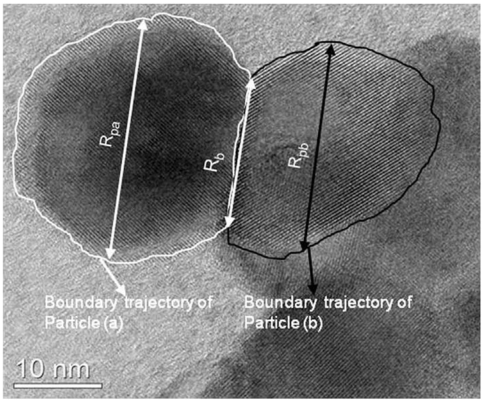

Fig. 7. Definition for inter-particle bonding ratio.(R_{Pa} refers to the diameter of the particle a; R_{Pb} refers to the diameter of the particle b; R_b refers to the diameter of inter-particle bonding boundary.).

Knowing this phenomenon, we can provide evident particle bonding by HR-TEM, as shown in Fig. 6(b)–(d). From the HR-TEM images, well-defined lattice fringes can be identified as the TiO_2 particles, and those nanoparticles are irregular shapes with surface roughness around 1–3 nm. It is reported that two nanoparticles were regarded as bonded together if their boundaries distance is less than a lattice parameter [32–34]. Therefore, two nanoparticles as shown in Fig. 6(b) are obviously bonded together after high velocity collision at ambient temperature and the boundary of the bonded particles is a step-like structure. Similarly, the HR-TEM images in Fig. 6(c) clearly show that clear bonding boundaries are formed at the interface under the collision at the particle temperature of 350 °C. This inter-particle bonding seems better than that at ambient temperature, which is similar with the microstructure of inter-particle bonding in the high-temperature processed coating following conventional sintering as shown in Fig. 6(d).

3.4. Quantitative examination the nano-sized particle bonding

To quantitatively examine the inter-particle bonding quality, a bonding ratio should be properly defined through the TEM image. In previous literature, α neck [41] and the distance of mass center of the bonded particles [34] were applied to characterize the inter-particle bonding, which is based on the assumption of the particles as regular spheres. However, TEM images show that most of TiO_2 particles have different diameters with a size distribution and particles have irregular shapes as shown in Fig. 7.

To define a more precise bonding ratio of bonded particles of TEM image, we firstly draw a boundary trajectory for each particle. Then, it was supposed that the width of the boundary trajectory was equal to the lattice parameter. The length of bonding neck for two particles was considered as a bonding region diameter, and parallel lines along with the bonding diameter in the particles were considered as the particles' diameter as shown in Fig. 7. The bonding ratio of bonded particles can be well defined as follows equation:

$$\text{Bonding ratio} = \frac{1}{2}\left[\left(\frac{R_b}{R_{Pa}}\right)^2 + \left(\frac{R_b}{R_{Pb}}\right)^2\right] \quad (1)$$

To make sure the reliability of this approach, the particle diameter was statistically examined. Results show that the particle diameter ranged from 5 to 50 nm with a mean size of 21.6 nm, which was near to the nominal diameter of 25 nm. This fact indicates that this approach is reliable for the estimation of the inter-particle bonding ratio of TEM image.

To precisely obtain the bonding ratio of TEM images, at least 50 pairs of bonded particles were examined and their bonding ratios were statistically estimated (as shown in Fig. 7). Fig. 8 shows that the bonding ratio for high temperature was higher than that for ambient temperature. This result was consistent with the performance of the dye-sensitized solar cells that electron transport resistance for the film deposited at high temperature is lower than low temperature resulting in a higher performance [35,36]. Those results indicate that ceramic nano-particles can be bonded together by a high velocity collision and the bonding ratio is increased with the increase of particle temperature. This result is consistent with the simulation results that particles temperature improved the particles bonding formation.

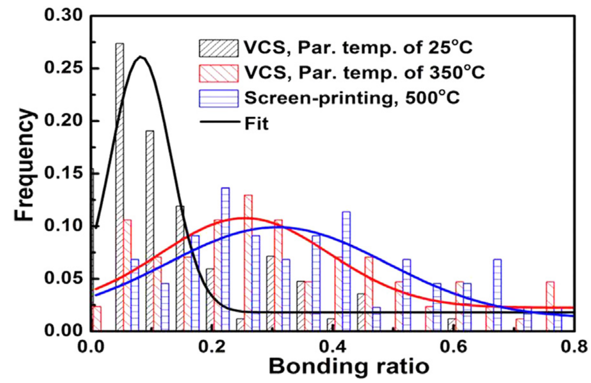

Fig. 8. Bonding ratios of nano-sized TiO_2 particles deposited by different approaches.

3.5. Bonding mechanisms for solid-state nano-sized TiO_2 particles

Nano-scale ceramic exhibits different deformation behavior from their bulk counterparts. In uniaxial compression tests, a size-dependent brittle-to-ductile transition for small-scale ceramic can be realized [17,18]. It was reported that the plastic deformation of bulk single crystals of TiO_2 (8 mm high by 3 × 3 mm cross-section) is possible at temperature above 600 °C [42]. The size-dependent brittle-to-ductile transition implies that plastic deformation of small TiO_2 single crystals is possible at a low temperature. Furthermore, results obtained by HR-TEM images show that nano-scale asperities present around the surfaces of TiO_2 particles (as shown in Fig. 6(b–d)). Although the incident speed is not high enough to cause bulk plastic deformation, the incident speed may be sufficient to cause deformation of those local asperities [14,39,43–45]. This fact indicated that the asperities around TiO_2 particles surface could be deformed under the high impact pressure as shown in Fig. 9. As consequently, nano-scale TiO_2 particles are bonded together by the high velocity collision at ambient temperature. This is different from many reported results present that submicron/micron-sized ceramic particles are always fragmented and crashed after high velocity collision [3–5,20–22]. Those literatures suggest that submicron/micron-sized ceramic particles are bonded together due to the fragments or amorphous induced by collision. Obviously, the nano-sized TiO_2 particle retained its integrity after high velocity collision as shown in Fig. 6. Furthermore, since the particle temperature increase

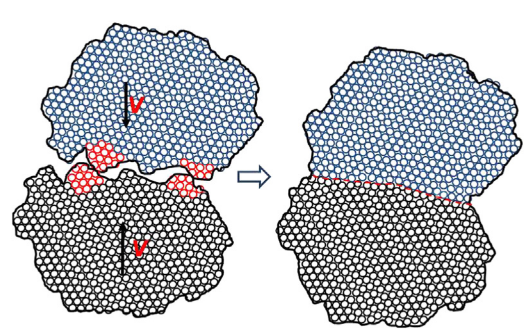

Fig. 9. Schematic diagrams of bonding formation.

during the collision, the deformation of the TiO_2 nano-particles becomes more easily at high velocity collision with a high particle temperature. The bonding formation induced by collision at high particle temperature is comparable to that for sintering at a high temperature and is higher than that by collision at ambient temperature (as shown in Fig. 6(b–d)). Those results indicate that nano-scale ceramic particles can be bonded together at a high velocity collision if having enough rough surface structures. TiO_2 nanoparticles could be bonded together by a high velocity collision due to the atomic displacements in the local region.

4. Conclusion

In conclusion, we have discovered a novel plastic deformation mechanism of nano-scale ceramic particle bonding formation derived by high velocity collision via MD simulation and TEM micro structural characterization. Simulation results demonstrate that the bonding formation of nano-sized TiO_2 particles can be attributed to the displacement and lattice distortion in localized impact region of particle boundaries. TEM microstructure results prove simulation results and indicate effective chemical bonding formations between nano-particles at low temperature by high velocity collision. Quantitative results show that the high temperature is beneficial to the particle bonding formation. The asperity around nano-sized ceramic particles surface contributed to the displacement and lattice distortion in localized impact region under the high impact compressive pressure. Therefore, being different from conventional dislocation slip, the present study demonstrates a new mechanism of nano-scale ceramic particle bonding formation induced by the localized atom displacement. Our study opens up a promising prospect of fabricating functional equipment with nano-scale ceramic particles with high velocity collision at ambient temperature.

Acknowledgements

The work is supported by the National Natural Science Foundation of China (No. 51072160), Program for New Century Excellent Talents in University (No. NCET-08–0443), Supported by State Key Laboratory for Mechanical Behavior of Materials (No. 20171911), Science and Technology Planning Progarm of Jiangxi Provincial Education Department (No. GJJ161068) and National Program for Support of Top-notch Young Professionals, Science and Technology Planning Program of Jiangxi Provincial Education Department.

References

[1] D. Hanft, J. Exner, M. Schubert, T. Stocker, P. Fuierer, R. Moos, An overview of the aerosol deposition method: process fundamentals and new trends in materials applications, J. Ceram. Sci. Technol. 6 (2015) 147–181.
[2] L. Zhu, T.C. Jen, Y.T. Pan, H.S. Chen, Particle bonding mechanism in cold gas dynamic spray: a three-dimensional approach, J. Therm. Spray. Technol. 26 (2017) 1859–1873.
[3] H. Assadi, F. Gertner, T. Stoltenhoff, H. Kreye, Bonding mechanism in cold gas spraying, Acta Mater. 51 (2003) 4379–4394.
[4] M. Isaza-Ruiz, J. Henon, O. Durand-Panteix, G. Etchegoyen, F. Rossignol, P. Marchet, Elaboration of lead-free $Na_{0.5}Bi_{0.5}TiO_3$-$BaTiO_3$ (NBT-BT) thick films by aerosol deposition method (ADM), Ceram. Int. 42 (2016) 14635–14641.
[5] Y. Imanaka, H. Amada, F. Kumasaka, N. Awaji, A. Kumamoto, Nanoparticulate $BaTiO_3$ film produced by aerosol-type nanoparticle deposition, J. Nanopart. Res. 18 (2016).
[6] H.S. Yun, J.C. Kim, D.Y. Jeong, N.H. Cho, Effect of nanoscale powders and microwave sintering on densification of alumina ceramics, Met. Mater. Int. 22 (2016) 1108–1115.
[7] A.C. Santos, S. Ribeiro, Liquid phase sintering and characterization of SiC ceramics, Ceram. Int. 44 (2018) 11048–11059.
[8] V. Prajzler, D. Salamon, K. Maca, Pressure-less rapid rate sintering of pre-sintered alumina and zirconia ceramics, Ceram. Int. 44 (2018) 10840–10846.
[9] C. Stampfl, A.J. Freeman, Stable and metastable structures of the multiphase tantalum nitride system, Phys. Rev. B 71 (2005).
[10] E. Murad, J. Cashion, Metastable Materials, Springer, US, 2004.
[11] G.X. Cao, D.J. Singh, X.G. Zhang, G. Samolyuk, L. Qiao, C. Parish, K. Jin, Y.W. Zhang, H.W. Guo, S.W. Tang, W.B. Wang, J.Y. Yi, C. Cantoni, W. Siemons, E.A. Payzant, M. Biegalski, T.Z. Ward, D. Mandrus, G.M. Stocks, Z. Gai, Ferromagnetism and nonmetallic transport of thin-film alpha-$FeSi_2$: a stabilized metastable material, Phys. Rev. Lett. 114 (2015).
[12] H. Zhang, A. Shan, L. Wei, W.U. Jiansheng, J. Zhang, Y. Liang, H. Song, Developments of the bonding mechanism and process in cold gas dynamic spray, Mater. Rev. 21 (2007) 80–84.
[13] Q. Wang, J.J. Liu, Y.F. Ye, T.T. Liu, S. Wang, C.T. Liu, J. Lu, Y. Yang, Universal secondary relaxation and unusual brittle-to-ductile transition in metallic glasses, Mater. Today 20 (2017) 293–300.
[14] J.H. Luo, J.W. Wang, E. Bitzek, J.Y. Huang, H. Zheng, L.M. Tong, Q. Yang, J. Li, S.X. Mao, Size-dependent brittle-to-ductile transition in silica glass anofibers, Nano Lett. 16 (2016) 105–113.
[15] L.E. Ferri, K.C. Hoff, S.P. Baker, Double-torsion measurements of the brittle-to-ductile transition temperature in calcium aluminosilicate glasses, Int. J. Appl. Glass Sci. 7 (2016) 532–544.
[16] A.K.M.N. Amin, M.N. Bagum, N. Fathiah, M. Konneh, T.F.B.M. Ariff, An experimental approach to determine the critical depth of cut in brittle-to-ductile phase transition during end milling of soda-lime glass, Arab. J. Sci. Eng. 41 (2016) 4553–4562.
[17] J. Wang, Y.G. Shen, F. Song, F.J. Ke, Y.L. Bai, C. Lu, Size-dependent brittle-to-ductile transition in GaAs nano-rods, Eng. Fract. Mech. 150 (2015) 135–142.
[18] F.L. Yuan, L.P. Huang, Brittle to ductile transition in densified silica glass, Sci. Rep. 4 (2014).
[19] M.M. Smedskjaer, Indentation size effect and the plastic compressibility of glass, Appl. Phys. Lett. 104 (2014).
[20] Y. Liu, Y.Y. Wang, X.K. Suo, Y.F. Gong, C.J. Li, H. Li, Impact-induced bonding and boundary amorphization of TiN ceramic particles during room temperature vacuum cold spray deposition, Ceram. Int. 42 (2016) 1640–1647.
[21] H. Park, J. Kwon, I. Lee, C. Lee, Shock-induced plasticity and fragmentation phenomena during alumina deposition in the vacuum kinetic spraying process, Scr. Mater. 100 (2015) 44–47.
[22] P. Sarobol, M. Chandross, J.D. Carroll, W.M. Mook, D.C. Bufford, B.L. Boyce, K. Hattar, P.G. Kotula, A.C. Hall, Room temperature deformation mechanisms of alumina particles observed from in situ micro-compression and atomistic simulations, J. Therm. Spray. Technol. 25 (2016) 82–93.
[23] W.M. Kang, M.T.A. Saif, In situ study of size and temperature dependent brittle-to-ductile transition in single crystal silicon, Adv. Funct. Mater. 23 (2013) 713–719.
[24] A. Montagne, S. Pathak, X. Maeder, J. Michler, Plasticity and fracture of sapphire at room temperature: load-controlled microcompression of four different orientations, Ceram. Int. 40 (2014) 2083–2090.
[25] J.W. Wang, Z. Zeng, C.R. Weinberger, Z. Zhang, T. Zhu, S.X. Mao, In situ atomic-scale observation of twinning-dominated deformation in nanoscale body-centred cubic tungsten, Nat. Mater. 14 (2015) 594–600.
[26] Y.J. Wang, K. Tsuchiya, L.H. Dai, Size-dependent plastic deformation and failure mechanisms of nanotwinned Ni_3Al: insights from an atomistic cracking model, Mater. Sci. Eng. a-Struct. Mater. Prop. Microstruct. Process. 649 (2016) 449–460.
[27] X. Li, H. Gao, Mechanical metamaterials: smaller and stronger, Nat. Mater. 15 (2016) 373.
[28] M.D. Uchic, D.M. Dimiduk, J.N. Florando, W.D. Nix, Sample dimensions influence strength and crystal plasticity, Science 305 (2004) 986.
[29] W.Z. Han, L. Huang, S. Ogata, H. Kimizuka, Z.C. Yang, C. Weinberger, Q.J. Li, B.Y. Liu, X.X. Zhang, J. Li, E. Ma, Z.W. Shan, From "Smaller is Stronger" to "Size-Independent Strength Plateau": towards measuring the ideal strength of iron, Adv. Mater. 27 (2015) 3385–3390.
[30] J.W. Wang, F. Sansoz, C. Deng, G. Xu, G.R. Han, S.X. Mao, Strong Hall-Petch type behavior in the elastic strain limit of nanotwinned gold nanowires, Nano Lett. 15 (2015) 3865–3870.
[31] C.C. Wang, J. Ding, Y.Q. Cheng, J.C. Wan, L. Tian, J. Sun, Z.W. Shan, J. Li, E. Ma, Sample size matters for $Al_{88}Fe_7Gd_5$ metallic glass: smaller is stronger, Acta Mater. 60 (2012) 5370–5379.
[32] Q. Mao, K.H. Luo, Molecular dynamics simulation of sintering dynamics of many TiO nanoparticles, J. Stat. Phys. 160 (2015) 1696–1708.
[33] B. Buesser, A.J. Grohn, S.E. Pratsinis, Sintering rate and mechanism of TiO_2 nanoparticles by molecular dynamics, J. Phys. Chem. C. 115 (2011) 11030–11035.
[34] V.N. Koparde, P.T. Cummings, Molecular dynamics simulation of titanium dioxide nanoparticle sintering, J. Phys. Chem. B 109 (2005) 24280–24287.
[35] H.L. Yao, G.J. Yang, S. Li, X.L. He, S.Q. Fan, C.X. Li, C.J. Li, Synergistic effects of high temperature and impact compaction on the Nano-TiO_2 film for the significant improvement of photovoltaic performance of flexible dye-sensitized solar cells, Electrochim. Acta 87 (2013) 940–947.
[36] N.G. Park, G. Schlichtherl, J.V.D. Lagemaat, H.M. Cheong, A.A. Mascarenhas, A.J. Frank, Dye-sensitized TiO_2 solar cells: structural and photoelectrochemical characterization of nanocrystalline electrodes formed from the hydrolysis of $TiCl_4$, Cheminform 30 (2016) (no-no).
[37] Q.Q. Qin, S. Yin, G.M. Cheng, X.Y. Li, T.H. Chang, G. Richter, Y. Zhu, H.J. Gao, Recoverable plasticity in penta-twinned metallic nanowires governed by dislocation nucleation and retraction, Nat. Commun. 6 (2015).
[38] L. Tian, J. Li, J. Sun, E. Ma, Z.W. Shan, Visualizing size-dependent deformation mechanism transition in Sn, Sci. Rep. 3 (2013) 2113.
[39] J. Sun, L.B. He, Y.C. Lo, T. Xu, H.C. Bi, L.T. Sun, Z. Zhang, S.X. Mao, J. Li, Liquid-like pseudoelasticity of sub-10 nm crystalline silver particles, Nat. Mater. 13 (2014) 1007–1012.
[40] H.L. Yao, G.J. Yang, S.Q. Fan, C.X. Li, C.J. Li, Ceramic nano-particle/substrate interface bonding formation derived from dynamic mechanical force at room temperature: HRTEM examination, J. Therm. Spray. Technol. 24 (2015) 720–728.

[41] M.J. Cass, A.B. Walker, D. Martinez, L.M. Peter, Grain morphology and trapping effects on electron transport in dye-sensitized nanocrystalline solar cells, J. Phys. Chem. B 109 (11) (2005) 5100–5107.

[42] K.H.G. Ashbee, R.E. Smallman, The plastic deformation of titanium dioxide single crystals, Proc. R. Soc. A 274 (1963) 195–205.

[43] D. Mordehai, E. Rabkin, D.J. Srolovitz, Pseudoelastic deformation during nanoscale adhesive contact formation, Phys. Rev. Lett. 107 (2011).

[44] C.Y. Guan, D.U. Cheng-Wang, G.H. Liu, X.D. Bai, Y. Zhang, S.H. Yuan, Dynamic tribology of heterogeneous materials based on asperities tangential deformation, Sci. Technol. Eng. (2018).

[45] B. Weber, T. Suhina, T. Junge, L. Pastewka, A.M. Brouwer, D. Bonn, Molecular probes reveal deviations from Amontons‘ law in multi-asperity frictional contacts, Nat. Commun. 9 (2018).